JTTEE5 17:365–376
DOI: 10.1007/s11666-008-9183-3
1059-9630/$19.00 © ASM International

Artificial Neural Networks vs. Fuzzy Logic: Simple Tools to Predict and Control Complex Processes—Application to Plasma Spray Processes

Abdoul-Fatah Kanta, Ghislain Montavon, Michel Vardelle, Marie-Pierre Planche, Christopher C. Berndt, and Christian Coddet

(Submitted October 8, 2007; in revised form January 13, 2008)

The plasma-sprayed coating architecture and in-service properties are derived from an amalgamation of intrinsic and extrinsic spray parameters. These parameters are interrelated; following mostly non-linear relationships. For example, adjusting power parameters (to modify particle temperature and velocity upon impact) also implies an adjustment of the feedstock injection parameters in order to optimize geometric and kinematic parameters. Optimization of the operating parameters is a first step. Controlling these is a second step and consists of defining unique combinations of parameter sets and maintaining them as constant during the entire spray process. These unique combinations must be defined with regard to the in-service coating properties. Several groups of operating parameters control the plasma spray process; namely (i) extrinsic parameters that can be adjusted directly (e.g., the arc current intensity) and (ii) intrinsic parameters, such as the particle velocity or its temperature upon impact, that are indirectly adjusted. Artificial intelligence (AI) is a suitable approach to predict operating parameters to attain required coating characteristics. Artificial Neural Networks (ANN) and Fuzzy Logic (FL) were implemented to predict in-flight particles characteristics as a function of power process parameters. The so-predicted operating parameters resulting from both methods were compared. The spray parameters are also predicted as a function of achieving a specified hardness or a required porosity level. The predicted operating parameters were compared with the predicted in-flight particle characteristics. The specific case of the deposition of alumina-titania (Al_2O_3-TiO_2, 13% by weight) by APS is considered.

Keywords artificial neural networks, atmospheric plasma spray, fuzzy logic, hardness, porosity, predicting properties, process parameters

1. Introduction

The Atmospheric Plasma Spray (APS) process is beneficial to deposit a variety of powder materials at high deposition rates to form thick (i.e., 150–350 μm, average thickness) layers onto substrates of various nature, size, and shape. In this process, powder particles are transported to the plasma jet by a carrier gas, where they are melted and simultaneously accelerated toward a substrate. After impact onto the substrate, the particles spread and solidify to form lamellae, the stacking of which creates a spray bead, and the superimposition of many such beads establishes a continuous coating (Ref 1).

The coating quality depends on the characteristics of the substrate (topology, chemistry, etc.) and the impinging particle state (quantity of momentum, impact angle, viscosity, degree of melting, etc.) (Ref 2). In turn, the particle state is related to the particle injection (quantity of momentum, etc.) and to the plasma flow characteristics (mass enthalpy, velocity, coefficient of thermal transfer, etc.). The coating quality control generally considers the monitoring of the feedstock particle characteristics (i.e., velocity and surface temperature) before their impingement onto the substrate since these influence significantly the coating in-service properties (Ref 2) and the microstructural features. Among these features, hardness and porosity level are key parameters that describe the anisotropy of a sprayed coating architecture and, therefore, their materials properties. The material properties can as a consequence of these relationships be controlled by adjusting the operating parameters; namely the power parameters.

Abdoul-Fatah Kanta, Marie-Pierre Planche and **Christian Coddet,** LERMPS, Université de Technologie de Belfort-Montbéliard, site de Sévenans, 90010, Belfort cedex, France; **Ghislain Montavon** and **Michel Vardelle**, SPCTS—UMR CNRS 6638, Faculty of Sciences, University of Limoges, 123 avenue Albert Thomas, 87060, Limoges cedex, France; **Christopher C. Berndt**, IRIS, Faculty of Engineering and Industrial Sciences, Swinburne University of Technology, Hawthorn 3122, Australia; and **Christopher C. Berndt**, Department of Materials Science and Engineering, Stony Brook University, Stony Brook, NY 11794. Contact e-mails: abdoul-fatah.kanta@utbm.fr and ghislain.montavon@unilim.fr.

Acronyms and Definitions	
AI	Artificial Intelligence: study and design of systems capable of perceiving their environment and taking actions maximizing their chance of success
ANN	Artificial Neural Network: interconnected group of artificial neurons which processes information using a connectionist approach to computation
Artificial neuron	(related to Artificial Neural Network) basic unit in an artificial neural network based on an abstraction of a biological neuron and which receives one or more inputs (representing the one or more dendrites) and sums them to produce an output (synapse). The sums of each node are weighted and the sum is passed through a non-linear function known as transfer function
Back-propagation	(related to Artificial Neural Network) most used technique used for training feed-forward artificial neural networks (networks that have no feedback or no connections that loop)
Defuzzification	(related to Fuzzy Logic) procedure during which a real value from the result of the inference is produced and can be used as a fuzzy control input
FL	Fuzzy Logic: derived from fuzzy set theory dealing with reasoning that is approximate rather than precisely deduced from classical predicate logic
Fuzzification	(related to Fuzzy Logic) procedure during which the real input variables (power parameters in the present study) are translated in terms of fuzzy sets
MF	Membership Function (related to Fuzzy Logic): associates a weighting with each of the inputs that are processed, defines functional overlap between inputs, and ultimately determines an output response. In the present study, MF correspond to the power parameters

The interactions among the spray variables, however, render optimization and control of this process quite complex. Understanding relationships between coating properties and process parameters is mandatory to optimize the process technique and the product quality.

Artificial intelligence based on artificial neural networks (ANN) and fuzzy logic (FL) offers new insights for optimizing and prediction of materials properties of this process. Indeed, such methods are appropriate tools to study complex processes with parameter interdependencies (Ref 3). In addition, they have proven to be applicable to the domain of materials science (Ref 4) and to process development; especially in the case of thermal spraying (Ref 5-8).

This article develops a model-based estimation for the power parameters in the APS process. Two models based on ANN and FL were proposed to predict the influence of power process parameters (arc current intensity, total plasma gas flow rate, and hydrogen percentage) on the in-flight particle characteristics. As well, some coating properties (porosity and microhardness) were predicted as a function of the power parameters and the corresponding in-flight particle velocity and temperature. The specific case of the deposition of alumina-titania (Al_2O_3-TiO_2, 13% by weight) by APS was considered in this study.

2. Experiments

2.1 Experimental Design and Set-ups

Metco 130 (Sulzer-Metco, Wohlen, Switzerland) fused and crushed gray alumina-titania (Al_2O_3-TiO_2, 13% by weight) powder of particle size distribution (determined implementing a laser particle distribution analyzer) ranging from 1.0 μm (d_{10}) to 57.5 μm (d_{90}) μm and of average (d_{50}) diameter of 35.7 μm was selected as the feedstock.

A Sulzer F4-type atmospheric plasma torch (Sulzer-Metco, Wohlen, Switzerland) of 50 kW maximum operating power, equipped with a anode nozzle of 6-mm internal diameter, was selected to carry out the experiments. Coatings were sprayed onto 25 mm diameter and 20-mm thick button-type AISI 304L (stainless steel) samples. Prior to spraying, substrates were manually grit-blasted using white corundum (α-Al_2O_3) of average diameter ranging from 425 to 600 μm (supplier data, Saint-Gobain, Avignon, France). After grit-blasting, the substrate exhibited an average roughness (Ra) of 3.6 μm, average value, and a peak-to-valley height (Rz) of 31.0 μm, average value. Substrates were then degreased by immersion in acetone vapors.

Several sets of power parameters were defined to manufacture the coatings. These sets permitted evaluation of the selected process parameters on the coating properties. In this fashion, the effect of the arc current intensity was adjusted between 350 and 650 A by fixing, respectively, the hydrogen mass percentage and the total plasma mass gas flow rate at 1.25% (25% at volume percentage) and 72.3 g min^{-1} (50 Nl min^{-1} at volume flow rate). The effect of the total plasma gas flow rate was studied between values of 50–100 g min^{-1} (35–70 Nl min^{-1} at volume flow rate) by keeping the hydrogen mass percentage and the arc current intensity constant at 1.25% and 530 A, respectively. The effect of the hydrogen mass percentage was studied between 0.25% and 1.75% (5% to 35% at volume percentage); whereas the total plasma gas flow rate and the arc current intensity were kept constant at 72.3 g min^{-1} and 530 A, respectively. The carrier gas flow rate was systematically adjusted using a non-intrusive

Table 1 Experimental data

Arc current intensity I, A	Plasma gas mass flowrate Ar + H_2, g min^{-1}	Hydrogen mass percentage H_2/Ar, %	In-flight particle average temperature and associated standard deviation T, °C	In-flight particle average velocity and associated standard deviation V, m s^{-1}	Averagemicrohardness and associated standard deviation VHN, $VHN_{0.3kg\ f}$	Average porosity and associated standard deviation P, %
350	72.3	1.25	2318 ± 3	264 ± 8	845 ± 33	5.0 ± 1.5
450	72.3	1.25	2421 ± 4	285 ± 10	864 ± 20	4.6 ± 1.0
530	72.3	1.25	2458 ± 2	302 ± 7	883 ± 60	3.9 ± 0.7
600	72.3	1.50	2516 ± 3	307 ± 7	913 ± 53	4.2 ± 1.5
650	72.3	1.25	2515 ± 5	324 ± 6	1053 ± 53	3.7 ± 1.9
700	71.7	0.38	2396 ± 3	336 ± 6	847 ± 43	6.6 ± 1.5
530	50.0	1.25	2415 ± 4	251 ± 3	794 ± 51	4.3 ± 0.7
530	60.0	1.25	2429 ± 5	270 ± 7	856 ± 35	6.8 ± 3.5
530	80.0	1.25	2433 ± 7	313 ± 9	876 ± 38	6.9 ± 1.1
530	90.0	1.25	2433 ± 5	311 ± 8	830 ± 18	8.7 ± 2.5
530	100.0	1.25	2419 ± 7	348 ± 13	909 ± 75	9.0 ± 1.3
530	72.3	0.25	2302 ± 4	267 ± 6	626 ± 36	7.2 ± 1.1
530	72.3	0.50	2357 ± 3	299 ± 6	770 ± 23	5.5 ± 1.0
530	72.3	0.75	2389 ± 3	303 ± 9	862 ± 34	7.0 ± 1.2
530	72.3	1.00	2409 ± 5	301 ± 10	741 ± 167	4.8 ± 1.4
530	72.3	1.50	2441 ± 5	299 ± 7	949 ± 28	5.3 ± 1.8

Table 2 Reference spray operating parameters for Metco 130 with a F4 type spray gun

Processing parameters	Values
Feedstock injection distance (distance from the injector tip to the plasma gun centerline axis)	6 mm
Feedstock injector internal diameter	1.8 mm
Feedstock mass rate	22 g min^{-1}
Plasma gun scanning step	12 mm $pass^{-1}$
Spray distance	125 mm

diagnostic tool (CCD camera equipped with filters and a short, i.e., a few ms, aperture duration) for each spray parameter set to obtain an optimal particle trajectory within the plasma flow. The particles penetrated into warm core of the flow with a deviation angle of about 4 degree. The experiments were performed in a random order to ward against lurking variables, Table 1. The other parameters were maintained at reference values, Table 2.

Concomitantly to the manufacture of thick coatings, in-flight particle average characteristics (velocity and temperature) were monitored for several sets of operating parameters using a Spray-Watch system (Osier, Tampere, Finland) (Ref 9). The diagnostic protocol considered 60 images for each operating parameter set. Values were then adjusted and averaged, Table 1.

2.2 Coating Microstructural Analysis

After conventional metallographic preparation performed on automatic systems (sample cutting and sample polishing), coating characterization was performed on their cross-sections by Scanning Electron Microscopy (SEM) in the secondary electron (SE) mode, leading to a resolution of 0.2 μm. Figure 1 displays a typical Al_2O_3-13TiO_2 coating structure. Stereology was then implemented to calculate the porosity level for each sample

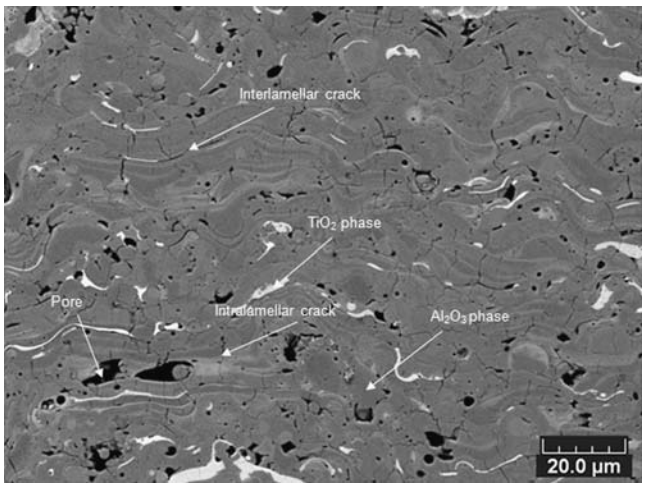

Fig. 1 Typical Al_2O_3-13TiO_2 coating cross-sectional structure

(Ref 10). Ten images, randomly captured along the cross-section, were analyzed per sample.

Vickers hardness measurements was performed on the polished cross-sections using a microhardness tester with a load of 300 g f and a dwell time of 15 s. Ten measurements randomly located along the cross-section were considered for each sample, the results being then averaged.

The experimental results are displayed in Table 1.

3. APS Process Simulation

3.1 Model Based on Fuzzy Logic

The FL concept was implemented to predict the in-flight particle characteristics (particle average velocity

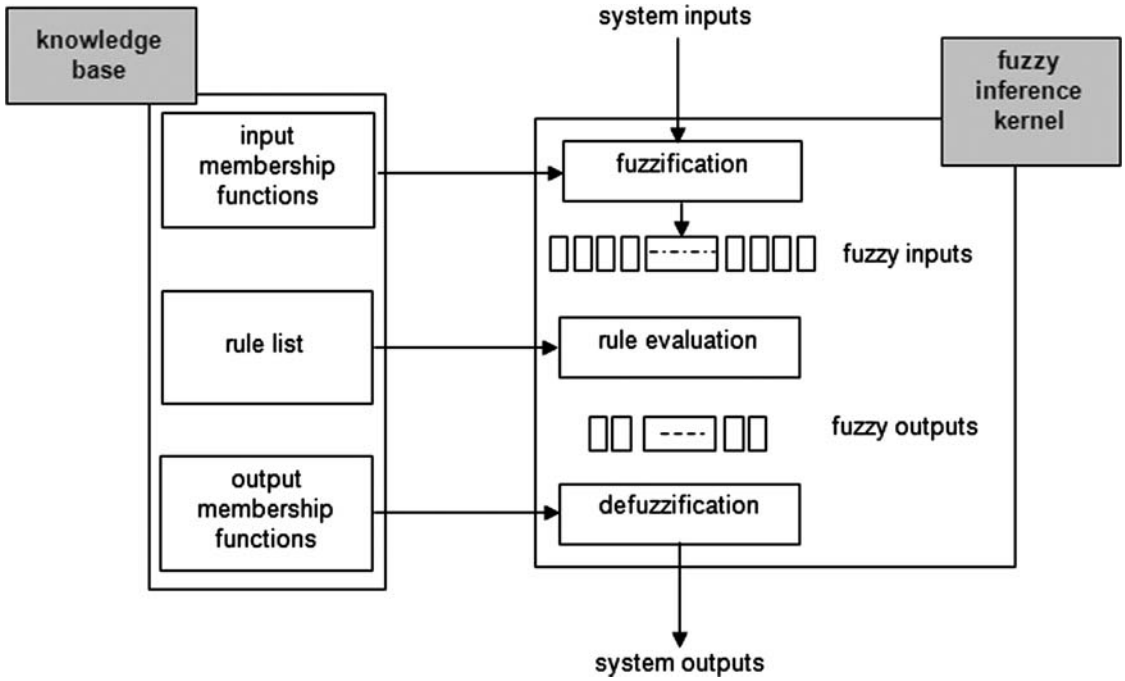

Fig. 2 Fuzzy logic basis system

and temperature) by varying three power-operating parameters. The model is empirically-based and permits a conclusion based upon imprecise input information, Fig. 2. The FL model is generally implemented following three successive steps, namely fuzzification, rule evaluation (or inference), and defuzzification (Ref 11).

3.1.1 Fuzzification and Membership Functions. The membership function (MF), corresponding in the present case to the power parameters, associates a weighting with each of the inputs that are processed, defines functional overlap between inputs, and ultimately determines an output response (Ref 12).

The fuzzification step translates real input variables (power parameters) into terms of fuzzy sets. A control algorithm is coded using fuzzy statements in the block containing the knowledge base by taking into account the objectives and the system behavior. Table 3 summarizes the considered process MF. This was achieved by evaluating all the input MF with respect to the current set of input values to establish the degree of activation of each MF. The true value for the premise of each rule was computed and applied to the conclusion part of each rule. These result in one fuzzy subset to be assigned to each output variable for each rule. Four MFs were employed to encode the inputs of the MF; these are:

- The symmetric Gaussian MF function that depends on two parameters, σ and c, as follows:

$$f(x, \sigma, c) = e^{\frac{-(x-c)^2}{2\sigma^2}} \quad \text{(Eq 1)}$$

The parameters for this function are the parameters σ and c listed in order in the vector [σ c].

Table 3 Power parameters (membership function, MF) decomposition

Level	Arc current intensity (I) parameter range: 200 → 900 A	Plasma forming gas flow rate (Ar + H_2) parameter range: 0 → 80 Nl min^{-1}	Hydrogen volume percentage (H_2/Ar) parameter range: 0 → 60%
Null	[200 300] (a)	[5 10] (a)	[10 10] (a)
Very low	[40 350] (c)	[15 20] (c)	[10 10] (c)
Low	[40 440] (c)	[15 35] (c)	[10 20] (c)
Medium	[40 530] (c)	[15 50] (c)	[10 35] (c)
High	[40 630] (c)	[15 65] (c)	[10 50] (c)
Very high	[530 750] (b)	[15 80] (b)	[10 60] (b)

(a) ZMF. (b) SMF. (c) Gauss MF

- The Z membership function (Z) is so named because of its Z shape. This spline-based function of x is depicted by:

$$\begin{Bmatrix} 1, x \le a \\ 1 - 2\left(\frac{x-a}{b-a}\right)^2, a \le x \le \frac{a+b}{2} \\ 2\left(\frac{b-x}{b-a}\right), \frac{a+b}{2} \le x \le b \\ 0, x \ge b \end{Bmatrix} \quad \text{(Eq 2)}$$

The parameters for Z membership function a and b locate the extremes of the sloped portion of the curve.

- The S membership function (S) is a spline-based curve that maps the vector x. The parameters for the

S membership function, a and b, locate the extremes of the sloped portion of the curve.

- The outputs MF, represent either the in-flight particle characteristics (average surface temperature and average velocity) and were selected as triangular functions; the characteristics of which were adjusted to describe the same tendencies as the ones of the experimental data. The triangular MF is a function of a vector, x, and depends on three scalar parameters a, b, and c, as given by:

$$f(x,a,b,c) = \max\left(\min\left(\frac{x-a}{b-a}, \frac{c-x}{c-b}\right), 0\right) \quad \text{(Eq 3)}$$

The parameters a and c locate the feet of the triangle and the parameter b locates the peak.

The selection of the MFs results from an optimization by trials and errors. Concerning the inputs, it appeared that symmetric Gaussian MFs presented the advantage to well describe the dispersions in the considered parameter values. S and Z MFs permitted to simply define the intervals over which parameters could not vary (corresponding to the process limits; *e.g.*, an arc current intensity lower than 300 A). Concerning the outputs, triangular MFs were selected since their use permitted to obtain the lowest possible differences between the predicted results and the reference values (i.e., experimental ones).

3.1.2 Rule Base. The rules use the input membership values as weighting factors to determine their influence on the fuzzy output sets of the final output conclusion. The truth value for the premise of each rule is computed and applied to the conclusion part of each rule. This results in one fuzzy subset that is assigned to each output variable for each rule. From the experimental database, different combinations between process parameters and in-flight particle characteristics permit determination of the fuzzy rules. Each rule is activated as soon as the membership degree of its premise is not null. Mamdani's rule (Ref 13) was used in this study; it can be expressed as follows:

$$\text{IF(I)is } A_1^i \text{ AND } (H_2 + Ar) \text{ is } A_2^i \text{ AND } (H_2/Ar) \text{ is } A_3^i \text{ THEN V is } B^i \text{ AND T is } C^i \quad \text{(Eq 4)}$$

The index "i" denotes input/output linguistic values from the fuzzy sets (very low, low, medium, high, very high). The terms A_1 A_2, A_3 are, respectively, associated to I, H_2 + Ar and H_2/Ar. V and T denotes in-flight particle velocity or surface temperature. B and C are the output linguistic values from the fuzzy set.

3.1.3 Inference Engine. The basic function of the inference engine is to compute the overall value of the fuzzy output based on the individual contributions of each rule in the rule base. Each individual contribution represents the value of the fuzzy output that is computed by a single rule. The inference method determines directly the outputs from the knowledge base and online data. Moreover, several rules can be activated simultaneously and recommend actions with various degrees of validities. These actions can be contradictory; in this case, it is advisable to aggregate the rules. The Max-Min composition (Ref 14) operation was used in this study.

3.1.4 Defuzzification. Defuzzification is the procedure that produces a real value from the result of the inference that could be used as a fuzzy control input. The set of modified control output values is converted into a single point wise value. This step produces a quantifiable result in FL. Characteristically, a fuzzy system will have a number of rules that transform a number of variables into a fuzzy result; thus the result is described in terms of membership in fuzzy sets. The defuzzification method that was used in this study is performed by combining the results of the inference process and by computing the fuzzy centroid of the area (Ref 15). The coordinate of the centroid corresponds to the defuzzified value and is expressed as follows:

$$\text{fuzzy output} = \frac{\int_U y \cdot \mu(y) \cdot dy}{\int_U \mu(y) \cdot dy} \quad \text{(Eq 5)}$$

where U represents all output values which are considered and y represents the output variable level and $\mu(y)$ the MF degree associate to y.

Based on Mamdani's implication for fuzzy inference reasoning, fuzzy rules (R_1, R_2, etc.) were established. An example of the rule-based array is illustrated in Fig. 3. The three inputs (I, H_2 + Ar, H_2/Ar) would be transformed into linguistic values; then the logic rules can be applied so that the linguistic and membership values for the outputs can be obtained.

3.2 Model Based on Artificial Neural Networks

The fundamental concept of neural networks concerns the structure of the information processing system. The neuron receives the weighted sum from the outputs of the other neurons and operates a non-linear transformation with the aid of a transfer function (Ref 16). In this study, the back-propagation algorithm was used (Ref 17). This is an established ANN technique for adjusting randomized weights during the data learning phase according to the steepest gradient along the error surface (Ref 18).

Experimental result sets have been organized in training and test samples of equal data set numbers. The training category was used to tune neural network weights and the test category to test the network configuration. To ensure that each input variable provides an equal contribution to the ANN, the input and output data were normalized previously to a common interval of [0,1] as follows (Ref 19):

$$x_{\text{normalised}} = \frac{x - \min(x)}{\max(x) - \min(x)} \quad \text{(Eq 6)}$$

where $x_{\text{normalized}}$ represented the formatted expression, and x the real value.

3.2.1 Training and Test Procedures. The training algorithms adopted in this study optimize the weights by minimizing the sum of squared differences between the desired (target values) and actual values (network value) of the output neurons (Eq. 1). While the training begins,

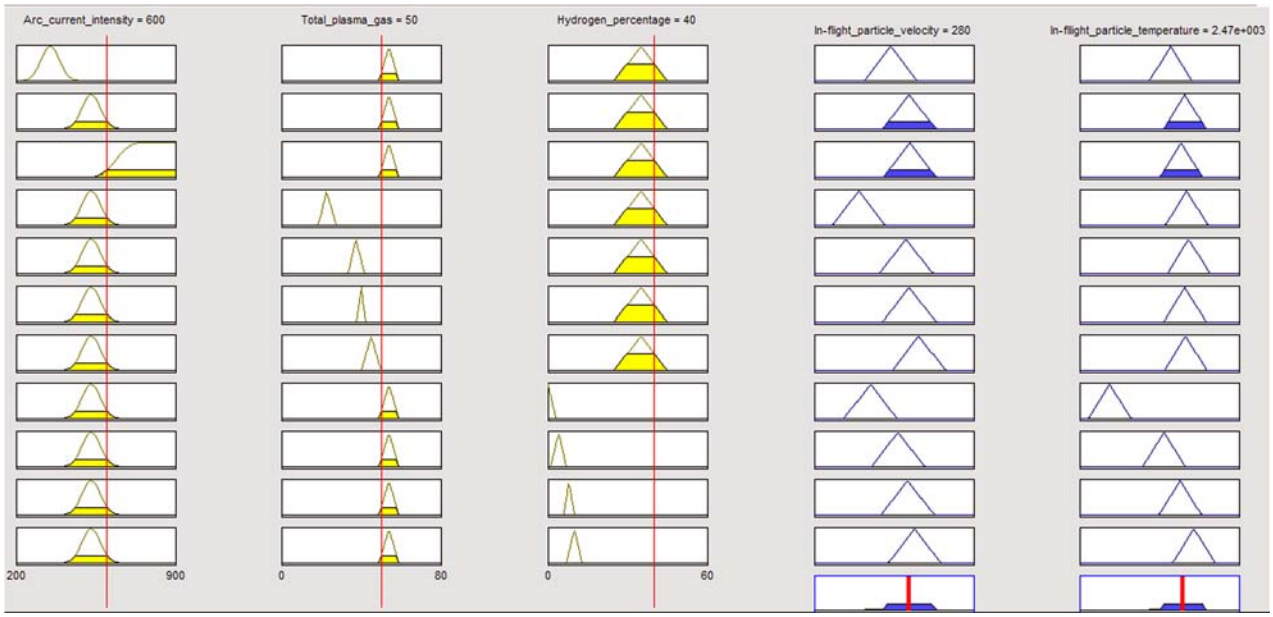

Fig. 3 Example of fuzzy logic reasoning

random weights (E) are assigned to all the connections as follows:

$$E = \frac{1}{2}\sum_{i=1}^{N}(y(k) - y_{net}(k))^2 \qquad \text{(Eq 7)}$$

where $y_{net}(k)$ is the network value and y(k) the target value.

The training algorithm continues backward through the hidden layers in the opposite direction, adjusting the values of the weights using a gradient descent method to reduce the error (Ref 20).

The weights are, hence, adjusted to reduce these prediction errors through a back propagation algorithm where the error is back distributed to the previous layers across the network. The optimization of the connection weights (w_{jk}) is performed according to:

$$w_{jk} = w_{jk}^{0} + \delta w_i \qquad \text{(Eq 8)}$$

where w_{jk}^{0} is the initial connection weight, $\delta w_i = -\mu \frac{\partial E}{\partial W_i}$ the weight correction and μ the learning rate.

After the training step, the model is tested using the test data to verify whether the network acquired source dynamics. If the network output for each test pattern is close to the respective target, the network is considered to have acquired the underlying dynamics from the training patterns (Ref 21).

3.2.2 Neural Networks Optimization. For the modeling process, user-defined parameters including the iteration number, the learning rate, momentum rate and the number of neurons in the hidden layer have to be determined and optimized. The optimization steps are detailed as:

- Formatting each variable of the database between 0 and 1.
- Dividing the database into two categories; (i) a training category required to tune weight population and (ii) a test category to test the validity of predicted results.
- Initializing the weight structure.
- Submitting a number of input/output examples to the structure from the database for training.
- Weighting values correction with the back-propagation method.
- Model testing (i.e., verification of its capacity to generalize the results): this step was performed at the end of the training procedure without modifying weight values.

The optimization of the ANN architecture was carried out using the optimal brain surgeon algorithm. The pruning procedure reduced the number of connections in all cases without performance degradation; but no significant improvement in the results was obtained. Also, this procedure reduces the calculation time. The performance of the ANN was evaluated with the Root Mean Square Error (RMSE) and the Mean Absolute Percentage Error (MAPE), as follows:

$$RMSE = \sqrt{\frac{1}{T}\sum_{k=1}^{k=T}(y_{net}(k) - y(k))^2} \qquad \text{(Eq 9)}$$

$$MAPE = \left[\frac{1}{T}\sum_{k=1}^{k=T}\frac{|y_{net}(k) - y(k)|}{y(k)}\right] \times 100\% \qquad \text{(Eq 10)}$$

where T is the highest value in the considered (training or test) dataset.

Root Mean Square Error and MAPE are the most widely used parameters to quantify ANN performance. They represent the fit between the neural network predictions and the actual targets. If the network outputs for each test pattern are relatively close to the respective targets, RMSE and MAPE exhibit small values and the network is considered to have acquired the underlying dynamics from the training patterns.

4. Results and Discussions

For defined processing parameters, the in-flight particle characteristics, and consequently the deposition properties, are mostly conditioned by the feedstock rate and the kinematic parameters (Ref 22). Discriminating the effect of each power process parameter is important to control the process. In order to validate the approach, the results need (i) to be consistent with experimental data and (ii) a large acceptance range is required.

4.1 Power Process Parameters Effect on the In-flight Particles Characteristics

The three considered ANN inputs to predict the in-flight particle average characteristics were the arc current intensity, the hydrogen mass percentage and the plasma forming gas total mass flow rate representing one neuron each. The two outputs were the in-flight particle average velocity and temperature, representing one neuron each as well. The optimal ANN structure, resulting from the optimization process, is composed of ten neurons in the hidden layer. The maximum values of MAPE and RSME were fixed, respectively, at 10% and 0.1. An optimized structure based on the experimental data was obtained after 10000 iterations of training and testing processes. The evolution of the convergence criterion is displayed in Fig. 4. The FL model rules are specifically defined for each case to optimize the response of the system. Each power process parameter was divided by level (Table 3) and each level was associated to the output MF. These considerations allow different combinations to be developed to determine the rule base. Many data can be introduced into the ANN model and, thus, the predicted result is represented in the form of a curve tendency, whereas in FL model, data are introduced just by single value and after defuzzification, the model gives the corresponding output.

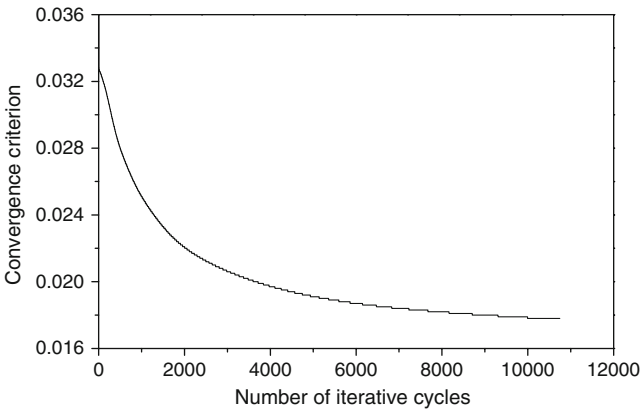

Fig. 4 Convergence criteria

The arc current intensity effect was studied between 350 and 650 A, the total plasma gas mass flow rate and the hydrogen mass percentage being fixed to 72.3 g.min^{-1} (50 Nl min^{-1} in volume flow rate) and 1.25% (25% in volume percentage), respectively. The results show that the in-flight particle average velocity and surface temperature increase, respectively, by 22% and 8% with the increase in the current intensity from 350 to 650 A, Fig. 5. The predicted results (ANN and FL) describe the same evolution as the experimental data. Concerning the ANN results, the prediction shows an increase of 22% and 7% for the in-flight particle average velocity and temperature, respectively, whereas this increase is about 22% and 9%, respectively, for the FL results, Table 4.

The evolution of in-flight particle characteristics were also studied while varying the hydrogen mass percentage between 0.25 and 1.50% (5–30% in volume ratio) and by fixing the total plasma gas mass flow rate to 72.3 g min^{-1} and the current intensity to 530 A. Figure 6 shows an increase in the in-flight particle average velocity and temperature. The predicted results indicate the same tendency. When the hydrogen mass percentage varied from 0.25 to 1.50%, the in-flight particle average velocity and temperature increase by 12% and 6%, respectively, Table 4. Hydrogen is a parameter that improves the thermodynamic properties of the jet; in particular by increasing the thermal conductivity and the enthalpy or by reducing the plasma jet viscosity (Ref 23).

Figure 7 shows the in-flight particle average characteristic evolution according to the total plasma gas mass flow rate that varied from 50 to 100 g min^{-1} (35–70 Nl min^{-1} in volume flow rate) while the hydrogen mass percentage was fixed to 1.25% (25% in volume percentage) and the current intensity to 530 A. The total plasma gas flow induced a significant increase in the particle velocity and a low variation in the particle temperature. Several studies confirm this tendency; see for example (Ref 24). The plasma energy and momentum transfer to the particles depend on their interaction duration and the gas nature. High thermal transfer is in particular required to obtain the highest possible number of particles completely melted on impact with the substrate. The energy contained in the plasma gas is released differently with the heat increase, according to whether diatomic or monoatomic plasma forming gases are considered. The addition of hydrogen as a secondary plasma forming gas to the primary argon plasma forming gas leads to an increase of the mixture enthalpy due to two mechanisms (Ref 25, 26):

1. Hydrogen molecular dissociation (around 3500 K) requires energy while pure argon begins to ionize only at 8000 K. Argon ionization becomes significant between 10000 and 15000 K; a temperature that is almost achieved (Ar and H exhibit ionization energies very close the one from the other: 15.8 and 13.6 eV, respectively);

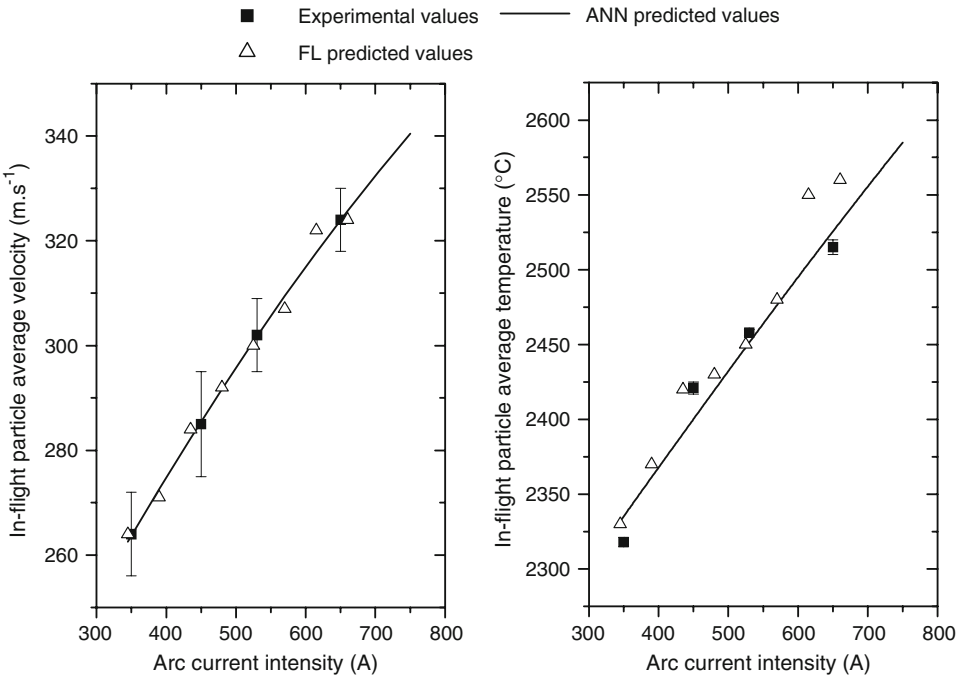

Fig. 5 Arc current intensity effect on in-flight particle average characteristics. Error bars represent standard deviation associated with experimentally determined average values

Table 4 Effect of power process parameters on in-flight particle average surface temperature and velocity

		Arc current intensity (I) when I increases from 350 to 650 A	Plasma forming gas mass flow rate ($Ar + H_2$) when $Ar + H_2$ increases from 50 to 100 g min^{-1}	Hydrogen mass percentage (H_2/Ar) when H_2/Ar increases from 0.25 to 1.50%
In-flight particle average temperature T	Exp	↑ 8.5%	↑ 0.7% then ↓ 0.6%	↑ 6%
	ANN	↑ 8.2%	↑ 0.7% then ↓ 0.9%	↑ 5.7%
	FL	↑ 9.9%	↑ 0.5% then →	↑ 4.7%
In-flight particle average velocity V	Exp	↑ 22.9%	↑ 38.7%	↑ 12%
	ANN	↑ 22.9%	↑ 35.7%	↑ 10.4%
	FL	↑ 22.3%	↑ 27.7%	↑ 7.5%

↓: Decreases by. ↑: Increases by. → : Does not vary

2. The plasma gas mixture specific mass is reduced by adding hydrogen (argon molecular weight is 40 g whereas hydrogen molecular weight is only 2 g, or in other words 1 kg of Ar represents 25 moles whereas 1 kg of H_2 represents 500 moles). Moreover, adding hydrogen leads to a drastic increase in the plasma mean integrated thermal conductivity. For example, considering a plasma temperature of 10000 K containing 20 vol.% of H_2, the mean integrated thermal conductivity is ~1 W m^{-1} K^{-1}; whereas it is below 0.2 W m^{-1} K^{-1} for pure argon plasma at the same reference temperature (Ref 27). The arc current intensity has a more pronounced effect on the in-flight particle average characteristics compared to the hydrogen percentage or the total plasma gas flow. The total plasma gas flow enables control of the particle mean velocity without changing significantly the temperature.

4.2 Deposit Structural Attributes

The required deposit structural attributes that were considered in this study are the total porosity level and the average coating microhardness (measured with a Vickers indenter). Tables 4, 5 summarized the effects of power process parameters on deposit characteristics that were determined experimentally. From the experimental data and implementing ANN protocols, the power parameters (arc current intensity, plasma forming gas mass total flow rate, hydrogen percentage) were predicted as a function of required deposit structural attributes (porosity level, Vickers hardness values). ANN was constituted by one input neuron corresponding to the considered deposit structural attribute and the output by three neurons corresponding to the power parameters that were predicted. After optimization, the ANN hidden layer was composed of 12 neurons. In parallel, another ANN composed of ten

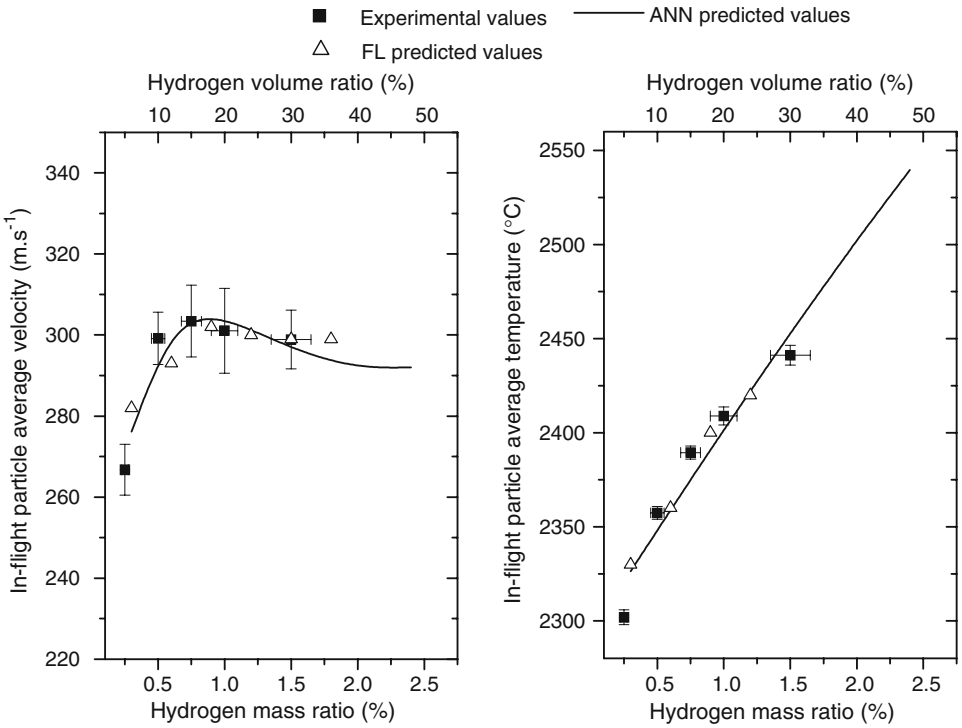

Fig. 6 Hydrogen percentage effect on in-flight particles characteristics. Error bars represent standard deviation associated with experimentally determined average values

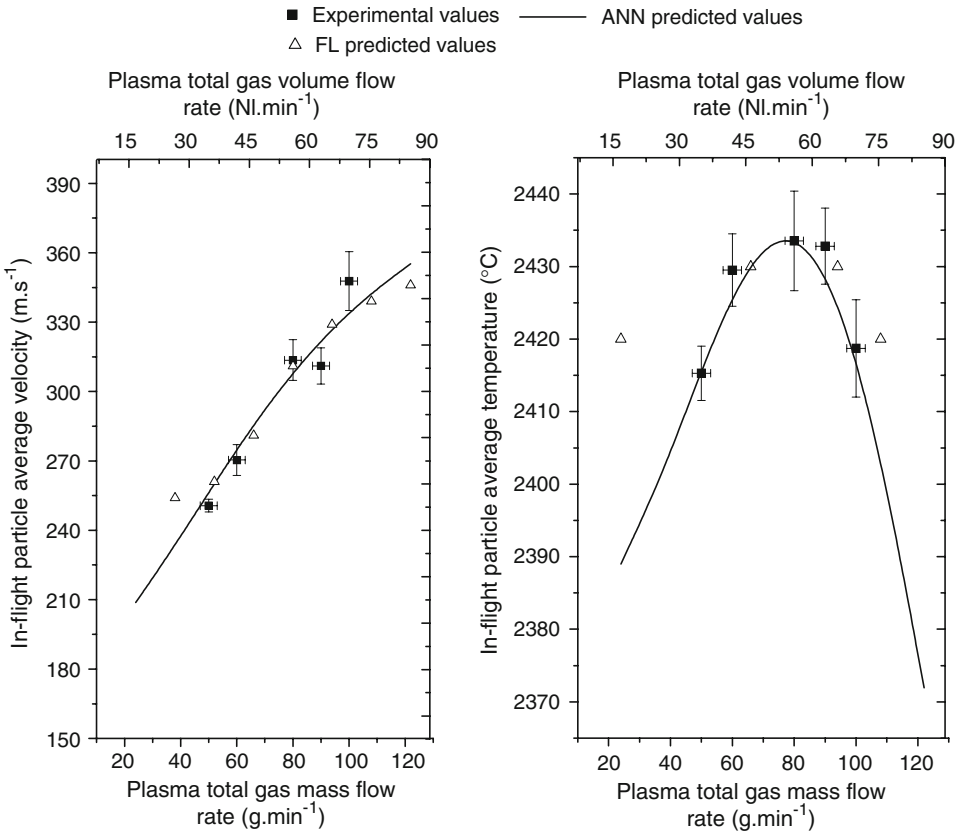

Fig. 7 Total plasma gas flow rate effect on in-flight particles characteristics. Error bars represent standard deviation associated with experimentally determined average values

neurons in its hidden layer (indeed, the first ANN structure that permitted prediction of particle average velocity and average surface temperature) was used to deduce the corresponding in-flight particle average characteristics for these predicted process parameters.

4.2.1 Deposit Hardness. Figure 8 shows the power parameters evolution vs. the deposit Vickers hardness value. For each considered power parameter, the two others were maintained at reference values (i.e., 530 A for arc current intensity, 72.3 g min^{-1} for plasma forming gas total mass flow rate and 1.25% for hydrogen mass percentage).

Over the studied range; the higher the required deposit hardness, the higher the power parameters. This corresponds to an increase in the in-flight particle characteristics, as illustrated in Fig. 9. A higher particle melting degree and a higher particle momentum upon impact are the required conditions to induce higher deposit cohesion, considering microhardness as a descriptor of the coating cohesion.

4.2.2 Deposit Porosity Level. An identical methodology was applied to predict power parameters and in-flight particle average characteristics vs. the required deposit porosity level.

The arc current intensity increases the plasma enthalpy and density of momentum quantity (Ref 2). Consequently an increase in the deposit porosity level requires a decrease in the arc current intensity, Fig. 10. Electric energy increases the in-flight particle average characteristics; thus the coating density (Ref 28). Figure 11 displays the corresponding in-flight particle characteristics. The hydrogen percentage has an effect on the porosity by modifying the plasma jet characteristics (Ref 23); i.e., the plasma enthalpy, its mean integrated thermal conductivity and its velocity increase while the plasma viscosity decreases. Even for low hydrogen mass percentage (less then 1%), hydrogen still improves the mean integrated thermal conductivity and promotes, hence, thermal exchange with the powder particles. For high hydrogen percentage, porosity does not vary significantly due to the fact that the enthalpy of the plasma jet reaches a critical value inducing significant feedstock evaporation (Ref 29). Friis et al. (Ref 30) have demonstrated the same evolution tendencies. In the same way, increasing the total mass rate of the plasma forming gas decreases molecular ionization and dissociation in the plasma jet (Ref 31). The particles are less heated before impact against the substrate (Ref 32); thus, the lamella flattening ratio decreases (Ref 33).

Table 5 Effect of power process parameters on deposit microhardness and porosity level

	Arc current intensity (I) when I increases from 350 to 650 A	Plasma forming gas mass flow rate ($Ar + H_2$) when $Ar + H_2$ increases from 50 to 100 g min^{-1}	Hydrogen mass percentage (H_2/Ar) when H_2/Ar increases from 0.25 to 1.50%
VHN	↑ 24.6%	↑ 14.5%	↑ 51.6%
P	↓ 26.8%	↑ 110.0%	↓ 26.2%

↓: decrease by. ↑: increase by. VHN: Vickers Hardness Number. P: pore level

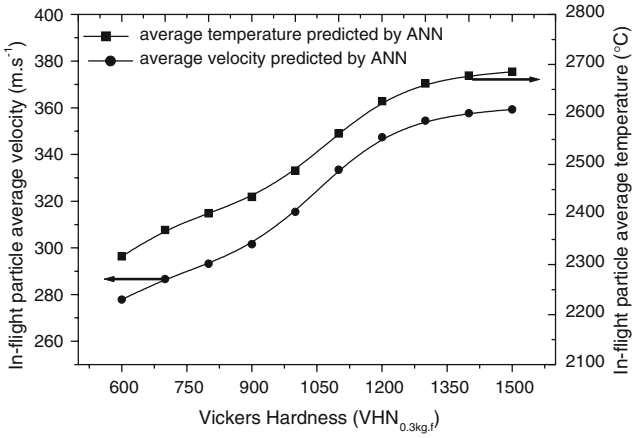

Fig. 9 Predicted particle in-flight particles characteristics vs. required deposit Vickers hardness value

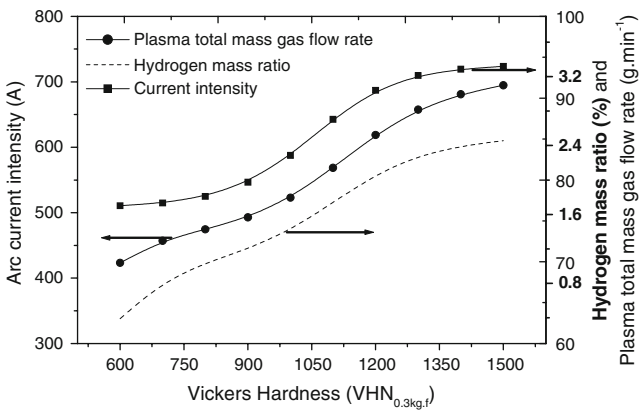

Fig. 8 Predicted power parameters vs. required deposit Vickers hardness value

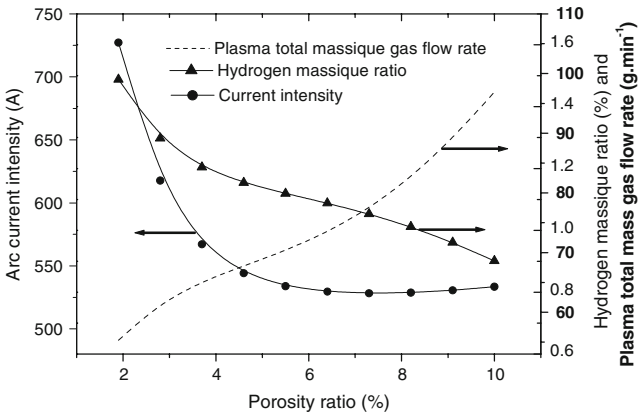

Fig. 10 Predicted power parameters vs. required deposit porosity level

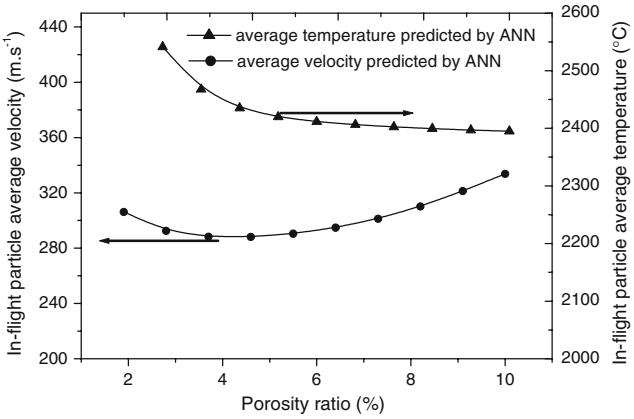

Fig. 11 Predicted particle in-flight particles characteristics vs. required deposit porosity level

Table 6 ANN and Fl method comparison

	FL	ANN
Uncertainty tolerance	+	++
Tolerance with the lack of precision	+	++
Adaptability	−	++
Training capacity	− −	++
Maintainability	+	++

− − Very bad, − Bad, + Good, ++ Very good

The plasma flow rate increases the particle average velocity and decreases their average temperature (Ref 2). Increasing this flow rate above a critical value leads to a decrease in the arc root diameter; reducing concomitantly the plasma flow core. Thus, only few particles will succeed in penetrating the reduced warm core region of the plasma jet; thus the particle temperature variation becomes insignificant for a porosity level higher than 6%.

Table 6 compares some criteria related to the ANN and FL models. From a general point of view, the ANN model appears more pertinent than the FL one with regard to the prediction and simulation concept. The ANN model is able to learn any behavior and its response can be updated/upgraded during using. The FL model is more suited for on-line control, since it delivers a response within a short time (Ref 34). These models have, hence, to be selected depending on the final purpose; i.e., process prediction (ANN) or process control (FL). With regard to thermal spray processing, AI is a good candidate for on-line control since it has the ability to model complex systems.

5. Conclusion

The power parameters are strongly correlated via mostly non-linear relationships. The influences of spray parameters on the in-flight particle average characteristics and the deposit structural attributes of alumina-titania coatings were investigated. Two models based on AI were implemented to understand and establish inter-relationships in the APS process. These models are a powerful technique that deliver a response within a very short time, once properly prepared.

The proposed model permits cost reduction *via* the possibility of adjusting the process parameter for each desired properties. The ANN model seems well adapted for process prediction; whereas the FL model appears more adapted for process control.

Acknowledgment

The French National Agency for Innovation (OSEO-ANVAR, grant number J 06.09.002 l) and the CNRS MRCT ''Plasma'' network are gratefully acknowledge for their financial support.

References

1. R.W. Smith and R. Knight, Thermal Spraying I: Powder Consolidation—From Coating to Forming, *J. Mater.*, 1995, **47**(8), p 32-39
2. M. Prystay, P. Gougeon, and C. Moreau, Structure of Plasma Sprayed Zircona Coatings Tailored by Controlling the Temperature and Velocity of the Sprayed Particles, *J. Therm. Spray Technol.*, 2001, **10**(1), p 67-75
3. M.M. Nelson and W.T. Illingworth, A Practical Guide to Neural Nets, 3rd Printing. Addison-Wesley, New York, 1991
4. H.K.D.H. Bhadeshia, Neural Networks in Materials Science, *ISIJ Int.*, 1999, **39**, p 966-979
5. S. Guessasma, G. Montavon, and C. Coddet, On the Neural Network Concept to Describe the Thermal Spray Deposition Process: Correlation Between In-flight Particles Characteristics and Processing Parameters, *Proceedings of the International Thermal Spray Conference 2002*, E.F. Lugcheider, Ed., (Düsseldorf), DVS-Verlag, 2002, p 435-440
6. M.-D. Jean, C.-D. Liub, and J.-T. Wang, Design and Development of Artificial Neural Networks for Depositing Powders in Coating Treatment, *Appl. Surf. Sci.*, 2005, **245**, p 290-303
7. M.-D. Jean, B.-T. Lin, and J.-H. Chou, Design of a Fuzzy Logic Approach Based on Genetic Algorithms for Robust Plasma-Sprayed Zirconia Depositions, *Acta Mater.*, 2007, **55**, p 1985-1997
8. M.-D. Jean, B.-T. Lin, and J.-H. Chou, Design of a Fuzzy Logic Approach for Optimization of Reinforced Zirconia Depositions Using Plasma Sprayings, *Surf. Coat. Technol.*, 2006, **201**, p 3129-3138
9. J. Vuttulainen, E. Hämäläinen, R. Hernberg, P. Vuoristo, and T. Müntyla, Novel Method for In-flight Particle Temperature and Velocity Measurements in Plasma Spraying Using a Single CCD Camera, *J. Therm. Spray Technol.*, 2001, **10**(1), p 94-104
10. S. Guessasma, G. Montavon, and C. Coddet, On the Implementation of the Fractal Concept to Quantify Thermal Spray Deposit Surface Characteristics, *Surf. Coat. Technol.*, 2003, **173**(1), p 24-38
11. S.O.T. Ogaji, L. Marinai, S. Sampath, R. Singh, and S.D. Prober, Gas-Turbine Fault Diagnostics: A Fuzzy-Logic Approach, *Appl. Energy.*, 2005, **82**(1), p 81-89
12. G. E. D'Errico, Fuzzy Control Systems with Application to Machining Processes, *J. Mater. Process. Technol.*, 2001, **109**, p 38-43
13. E.H. Mamdani and S. Assilian, An Experiment in Linguistic Synthesis with a Fuzzy Logic Controller, *Int. J. Man Mach. Stud.*, 1975, **7**(1), p 1-13
14. I. Eker and Y. Torun, Fuzzy Logic Control to be Conventional Method, *Energy Convers. Manag.*, 2006, **47**(4), p 377-394

15. T. Fraichard and P. Garnier, Fuzzy Control to Drive Car Like Vehicles, *Robot. Auton. Syst.*, 2001, **34**(1), p 1-22
16. D.T. Pham and L. Xing, Neural Networks for Identification, Prediction and Control, 2nd Printing. Springer, London, Great Britain, 1995
17. N.O. Attoh-Okine, Analysis of Learning Rate and Momentum Term in Back Propagation Neural Network Algorithm Trained to Predict Pavement Performance, *Adv. Eng. Softw.*, 1999, **30**(4), p 291-302
18. C.M. Bishop, Training with Noise Is Equivalent to Tikhonov Regularization, *Neural Comput.*, 1995, **7**(1), p 108-116
19. L.M. Romeo and R. Gareta, Neural Network for Evaluating Boiler Behaviour, *Appl. Therm. Eng.*, 2006, **26**, p 1530-1536
20. H.B. Celikoglu, Application of Radial Basis Functions and Generalized Regression Neural Networks in Non-Linear Utility Function Specification for Travel Mode Choice Modeling, *Math. Comput. Model.*, 2006, **44**, p 640-658
21. Y. Reich and S.V. Barai, Evaluating Machine Learning Models for Engineering Problems, *Artif. Intell. Eng.*, 1999, **13**(3), p 257-272
22. R. Kingswell, K.T. Scott, and L.L. Wassell, Optimizing the Vacuum Plasma Spray Deposition of Metal, Ceramic and Cermet Coatings Using Designed Experiments, *J. Therm. Spray Technol.*, 1993, **2**(2), p 179-186
23. E. Pfender, Fundamental Studies Associated with the Plasma Spray Process, *Surf. Coat. Technol.*, 1988, **34**(1), p 1-14
24. E. Lugscheider, A. Fischer, D. Koch, and N. Papenfub, Diagnostic of In-flight Particle Properties and Resulting Coating Qualities on Atmospheric Plasma Spray Process, *Thermal Spray 2001: New Surfaces for a New Millennium,* C.C. Berndt, K.A. Khor, and E.F. Lugscheider, Eds., Materials Park, OH, ASM International, 2001, p 751-758
25. M. Tului, F. Ruffni, F. Arezzo, S. Lasisz, Z. Znamirowski, and L. Pawlowski, Some Properties of Atmospheric Air and Inert Gas High-Pressure Plasma Sprayed ZrB_2 Coatings, *Surf. Coat. Technol.*, 2002, **151-152**, p 483-489
26. M. A. P. Vardelle Fauchais, Diagnostics for Particulate Vaporization and Interactions with Surfaces, *Pure Appl. Chem.*, 1992, **64**(5), p 637-644
27. J. Patru, Modélisation du développement des contraintes résiduelles au sein de dépôts plasma de zircone et d'acier (modeling of the development of reidual stresses within zircone and steel plasma-sprayed coatings), Ph.D. Thesis, n. 64, University of Limoges, France, 2005, in French
28. D.J. Varacalle, H. Herman, G.A. Bancke, and W.L. Riggs, Vacuum Plasma-Sprayed Alumina-Titania Coatings, *Surf. Coat. Technol.*, 1992, **54-55**, p 19-24
29. D.R. Marsh, N.E. Weare, and D.L. Walker, Process Variables in Plasma-Jet Spraying, *J. Met.*, 1961, **2**, p 473-478
30. M. Friis, C. Persson, and J. Wigren, Influence of Particle In-flight Characteristics on the Microstructure of Atmospheric Plasma Sprayed Yttria Stabilized ZrO_2, *Surf. Coat. Technol.*, 2001, **141**, p 115-127
31. I.A. Fisher, Variables Influencing the Characteristics of Plasma-Sprayed Coatings, *Int. Metall. Rev.*, 1972, **17**, p 117-136
32. T.J. Steeper, D.J. Varacalle, G.C. Wilson, W.L. Riggs, A.J. Rotolico, and J.E. Nerz, A Design of Experiment Study of Plasma Sprayed Alumina-Titania Coatings, *Thermal Spray: Advances in Coatings Technology,* C.C. Berndt, Ed., Materials Park, OH, ASM International, 1992, p 415-420
33. T.J. Steeper, A.J. Rotolico, J.E. Nerz, W.L. Riggs, D.J. Varacalle, and G.C. Wilson, A Tagushi Experimental Design Study of Plasma Sprayed Alumina-Titania Coatings, *Thermal Spray Coatings: Properties, Processes and Applications,* T.F. Bernecki, Ed., Materials Park, OH, ASM International, 1992, p 13-20
34. A.F. Kanta, G. Montavon, M.P. Planche, and C. Coddet, Plasma Spray Process on-Line Control by Artificial Intelligence Methodology, *Adv. Eng. Mater.*, 2007, **9**, p 105-113